PNAS
www.pnas.org

Supplementary Information for

Linkage between retinal ganglion cell density and the nonuniform spatial integration across the visual field

MiYoung Kwon, PhD[1] & Rong Liu, PhD[1]
[1]Department of Ophthalmology and Visual Sciences,
University of Alabama at Birmingham, Birmingham, AL

Correspondence: MiYoung Kwon
700 S. 18th Street, Suite 407 | Birmingham, AL 35294
Email: miyoungkwon02@gmail.com

This PDF file includes:

Supplementary Information Text

SUPPLEMENTAL METHODS

STIMULI AND TASK PROCEDURES

Measuring Ricco's area. The stimulus was an achromatic luminance disc (Fig. 2A) displayed on a uniform gray background (10 cd/m^2). The stimuli were generated and controlled using MATLAB (R2014b) and Psychophysics Toolbox extensions (1, 2) for Windows 7, running on a PC desktop computer (model: Dell Precision Tower 5810). The stimuli were rendered on a 32″ Display++ LCD monitor (Cambridge Research Systems, Ltd., UK) with the maximum brightness of 105 cd/m^2. The display had a refresh rate of 120 Hz and a resolution of 1920 × 1080 pixels. All the measurements were made at the viewing distance of 57 cm while the 4° eccentricity condition was measured at the viewing distance of 100 cm (This was done to match the spatial resolution capacity of the human parafoveal retina). The monitor was set to Mono++ mode to achieve up to 16-bit grayscale precision. Participants were seated in front of the display monitor in a dark room. A chin- and headrest was used to limit head movements and to maintain the constant viewing distance. Throughout each experimental session, the experimenter visually observed subjects to confirm that fixation instructions were followed.

A subject's task was to detect the target disc displayed on a computer screen. A subject's contrast detection threshold (expressed as Weber contrast) was measured with a temporal two-alternative forced-choice (2AFC) staircase procedure. A 3-down-1-up staircase with the step size of 1 dB was adopted, yielding a threshold criterion of 79.4% correct (3). The geometric mean of the last 8 out of 9 staircase reversals was taken as the threshold for each staircase run. In each trial, there were two 250-ms intervals each marked by an auditory beep, separated by 750 ms, one containing a target disc. A subject was asked to judge which stimulus interval contained a target disc by pressing one of two keys. At the beginning of each block, in order to cue subjects, a red line with the same length as the target diameter was shown at the target location. Auditory feedback was given whenever a correct answer was made. Thresholds were obtained for 6 different disc sizes ranging from 0.08° to 2° in diameter. Each disc size was tested in in a separate block and the order of disc sizes was randomized. Spatial summation curve (Fig. 2B), a plot of log contrast detection thresholds as a function of log stimulus area (deg^2), was fitted with two lines. To estimate Ricco's area, the slope of the first line was constrained to a value of -1 in accordance with Ricco's law, whereas the slope of the second line was allowed to vary. Ricco's area was defined as the breakpoint of the two-limbed function as shown in Fig. 2B. Ricco's area was measured at 7 different visual-field locations: four eccentricities (4°, 8.5°, 13.5° and 18.5° on the horizontal meridian) in the nasal visual field and three additional locations at the eccentricity of 8.5°. Each location can be denoted as (ρ, θ) in the polar coordinates: (4°, 180°), (8.5°, 180°), (13.5°, 180°), (18.5°, 180°), (8.5°, 0°), (8.5°, 90°), and (8.5°, 270°) if the subject's test eye is the right eye. Note that the data in the current study are all expressed in visual-field coordinates (i.e., Uvf, Lvf, Nvf and Tvf for the upper, lower, nasal and temporal visual field, respectively)

rather than retinal coordinates. Therefore, the data from the nasal visual field contain an individual subject's left or right visual-field data depending on his/her tested eye. The same applies to the data from the temporal visual field. Thus, regardless of the tested eye, the nasal visual field always corresponds to the subject's temporal retina; the temporal visual field corresponds to the subject's nasal retina; the upper visual field corresponds to the subject's inferior retina; and the lower visual field corresponds to the subject's superior retina.

Measuring critical spacing. The stimuli consisted of a target letter flanked by two tumbling Es appearing on both sides of the target along the radial axis. The target letter was randomly drawn from a set of 10 Sloan letters: CDHKNORSVZ. All the letters were white on a uniform gray background with a letter size of 1º (x-height). The same display apparatus and controlling system were used as Ricco's area. A subject's task was to judge the identity of the target letter flanked by two tumbling Es with a contrast of 0.85 (Fig. 2C). At the beginning of each block, a small red dot flanked by two gray dots was shown at the target location. In each trial, subjects were presented with a target letter for 250 ms followed by a blank interval (500 ms). Next, a set of 10 thumbnail versions of the letter images appeared on the screen. Subjects reported the identity of the target letter by clicking the mouse on one of 10-letter answering keys forming a clock face. Auditory feedback was given whenever a correct answer was made. A subject's letter-recognition contrast threshold was measured with the same 3-down-1-up staircase procedure described above, yielding a threshold criterion of 79.4% correct. The geometric mean of the last 6 out of 7 staircase reversals was taken as the threshold for each staircase run. Thresholds were obtained for 8 different spacings (i.e., the center-to-center distance between the target letter and flankers). Each spacing condition was tested in in a separate block and the order of spacings was randomized. Clipped lines were fitted to the data of log recognition threshold versus spacing. Critical spacing was defined as the minimum spacing (deg) that yields no threshold elevation in the fit (4). Critical spacing was measured at 7 different visual field locations as described in the Ricco's area section.

DATA ANALYSES

To examine the role of RGC density in the extent of spatial integration for human pattern vision, we estimated the number of RGCs underlying either Ricco's area or crowding zone for each target location (Fig. 2E):

i) Ricco's area (deg^2) for luminance detection and critical spacing (deg) for object recognition were obtained from the dominant eye of each normally-sighted subject.

ii) Each subject's critical spacing in a unit of length (deg) was converted into a corresponding unit of area (deg^2) for each target location. Considering the radial-tangential anisotropy of crowding zone (5-8), an elliptical shape was used for the area conversion. We computed the area of an ellipse with its major axis equals to twice the subject's critical spacing and its minor axis equals to the subject's critical spacing (5).

Crowding zone = $0.5 \times \pi \times$critical spacing^2 **(Eq. 1)**

iii) The RGC density corresponding to each target location in the visual field was derived from Drasdo et al.'s formula (9) based on RGC receptive field density after adjusting for RGC displacement in the adult human retina.

iv) The product of Ricco's area (deg^2) or crowding zone (deg^2) and RGC density (deg^{-2}) was computed for each target location. To be more precise, we calculated the integral of products of ΔRicco's area or Δcrowding zone and the corresponding RGC density over the entire integration zone (10). This was done to take into account that the RGC density varies continuously over the extent of Ricco's area or crowding zone.

v) This yields a plot of the number of RGCs as a function of target location. Depending on the patterns of the underlying RGC density, three hypothetical outcomes are expected: *Zero Contribution*, *Partial Contribution*, and *Full Contribution*.

vi) We then quantified the contribution of the RGC density by computing the amount of the variance that can be explained by the underlying RGC density with respect to the total variance (Eq. 2): a value of 0% means *Zero Contribution* whereas a value of 100% indicates *Full Contribution*.

$$\text{Contribution}(\%) = \frac{(RSS_{\text{ZeroContribution}} - RSS_{\text{ActualResults}})}{RSS_{\text{ZeroContribution}}} \times 100, \quad \textbf{(Eq. 2)}$$

where $RSS\ (Residual\ Sum\ of\ Squares) = \sum_{i=1}^{n}(y_i - \bar{y})^2$.

We also calculated the number of RGCs underlying crowding zone approximated by Bouma's law. In 1970, Bouma (11) reported that critical spacing was about 0.5 times the eccentricity of target ($y = 0.5$ *eccentricity*). In 1976, Andriessen and Bouma (12) reduced the estimate of the proportionality constant from 0.5 to 0.4. In our study, we chose 0.4 as the proportionality constant. The number of RGCs underlying crowding zone will differ depending on the proportionality constant of Bouma's law, whether it is 0.4 (12) or 0.5 (11). However, it should be noted that using a different coefficient value only results in a vertical shift of the resulting curve (i.e., a plot of the number of RGCs vs. eccentricity) without changing the shape of the curve. Therefore, using a different the proportionality constant does not make any difference as to our main point, whether the number of RGCs underlying eccentricity-dependent increase in crowding zone remains constant across eccentricities or not.

To determine whether there is any statistically significant difference in either the extent of spatial integration or the number of RGCs among target locations, we performed one-way repeated-measures ANOVA. The extent of spatial integration and number of RGCs data were all transformed into logarithmic units for the statistical analyses. To further determine which specific target location differs from each other, we also performed

contrast tests. Statistical analyses were performed using the *R* software (version 3.3.3) in combination with MATLAB (R2014b; MathWorks, Inc.).

SUPPLEMENTAL FIGURES

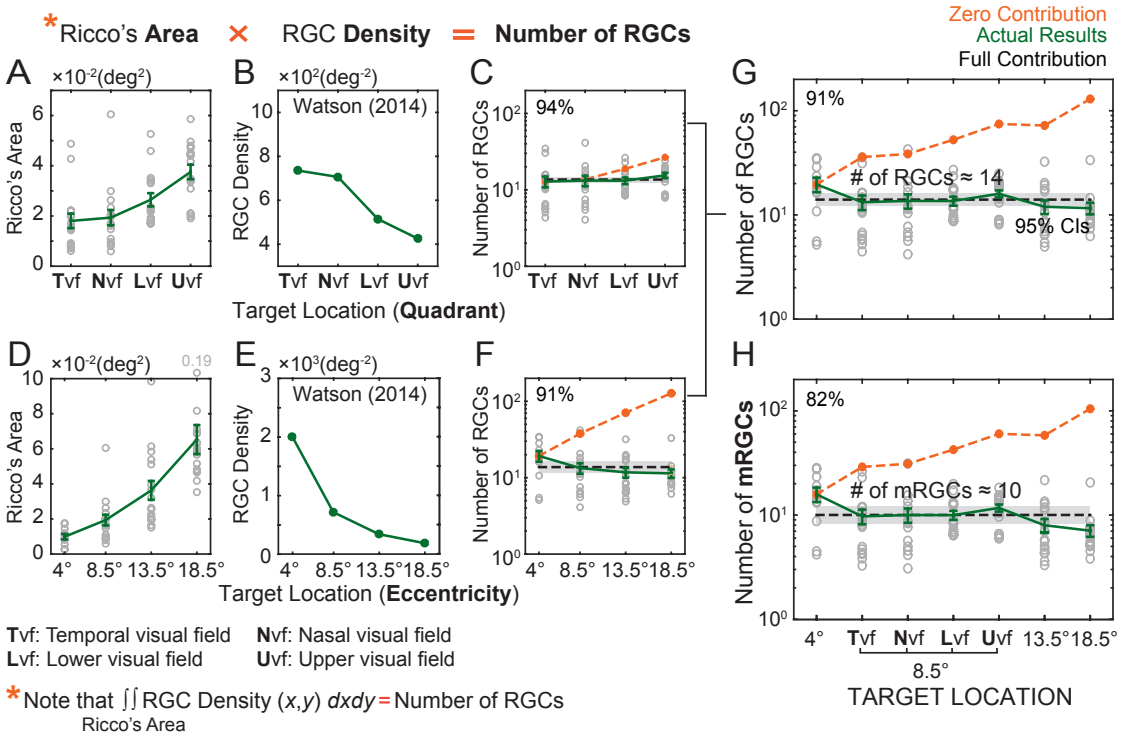

Fig. S1, Related to Fig. 3. Number of RGCs underlying Ricco's area using Watson's formula (10). A) Ricco's area is plotted as a function of visual-field quadrant. Gray open dots represent individual subjects' data points. The green solid line indicates the average Ricco's area across subjects for a given target location. Error bars represent ± 1 standard error of the mean (SEM). **B)** The RGC density (green solid line) estimated from the formula (10) is plotted as a function of visual-field quadrant. **C)** The number of RGCs (i.e., actual results indicated by green line) underlying Ricco's area, i.e., the product of Ricco's area (deg^2) and the RGC density (deg^{-2}), is plotted as a function of visual-field quadrant in comparison with *Zero Contribution* (orange dotted line) and *Full Contribution* (black dotted line) curves. Shaded gray areas indicate 95% Confidence Intervals (CIs) of *Full Contribution*. **D)** Ricco's area vs. visual-field eccentricity. **E)** The RGC density vs. eccentricity. **F)** The number of RGCs (i.e., actual results) underlying Ricco's area vs. eccentricity. **G)** The number of RGCs underlying Ricco's area is plotted as a function of target location in comparison with *Zero Contribution* and *Full Contribution* curves. **H)** The number of midget RGCs (mRGCs) underlying Ricco's area is plotted as a function of target location in comparison with *Zero Contribution* and *Full Contribution* curves.

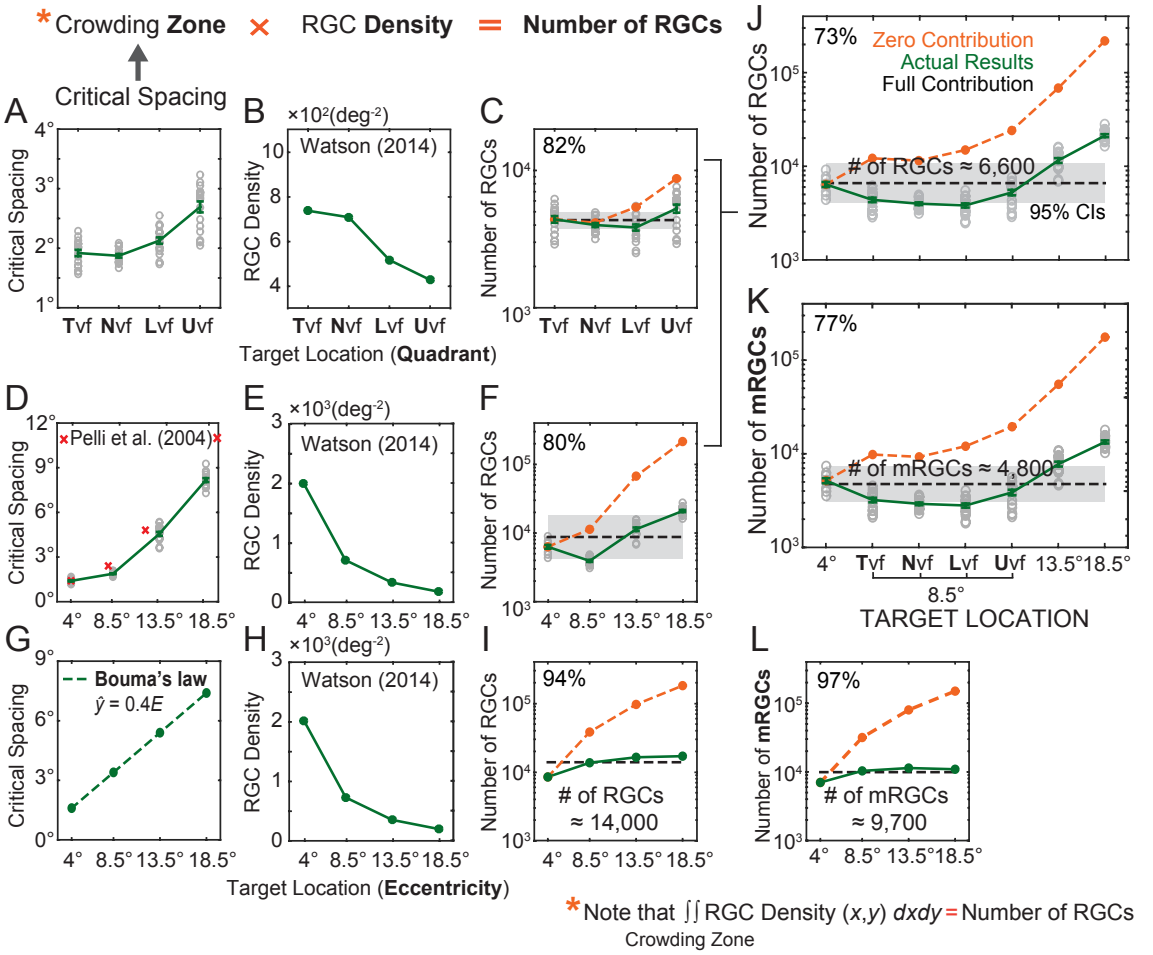

Fig. S2, Related to Fig. 4. Number of RGCs underlying crowding zone or Bouma's law of crowding using Watson's formula (10). A) Critical spacing (deg) is plotted as a function of visual-field quadrant. Gray open dots represent individual subjects' data points. The green solid line indicates the average critical spacing across subjects for a given target location. Error bars represent ± 1 SEM. **B)** The RGC density (green solid line) estimated from the formula (10) is plotted as a function of visual-field quadrant. **C)** The number of RGCs (i.e., actual results depicted by green line) underlying crowding zone, the product of crowding zone (deg^2) and the RGC density (deg^{-2}), is plotted as a function of visual-field quadrant in comparison with *Zero Contribution* (orange dotted line) and *Full Contribution* (black dotted line) curves. Shaded gray areas indicate 95% CIs of *Full Contribution.* **D)** Critical spacing vs. eccentricity data from our study (gray symbols) compared with the data (red crosses) from Pelli et al. (4). **E)** The RGC density vs. eccentricity. **F)** The number of RGCs (i.e., actual results) underlying crowding zone vs. eccentricity. **G)** Critical spacing predicted by Bouma's law is plotted against eccentricity. **H)** The RGC density vs. eccentricity. **I)** The number of RGCs underlying crowding zone predicted by Bouma's law is plotted against eccentricity in comparison with *Zero Contribution* and *Full Contribution* curves. **J)** The number of RGCs underlying crowding zone is plotted against target location in comparison with *Zero Contribution* and *Full Contribution* curves. **K)** The number of midget RGCs (mRGCs) underlying crowding zone is plotted against target location. **L)** The number of mRGCs underlying crowding zone predicted by Bouma's law is plotted against eccentricity.

SUPPLEMENTAL TABLES

Table S1, Related to the Methods. The number of participants (n) for each experimental condition

	Target location (ρ, θ)						
	(4°, 180°)	(8.5°, 0°)	(8.5°, 90°)	(8.5°, 180°)	(8.5°, 270°)	(13.5°, 180°)	(18.5°, 180°)
Ricco's area	11	17	17	17	17	17	17
Crowding zone	11	17	17	17	17	16	16

Table S2, Related to Fig. 3I. Parameter values of the Retina-V1 Detection Model

Parameter	k_c	k_s	w_c	ρ	P_0
Current study	1	2.6	0.46	2.0	0.0021
Bradley et al., 2014	1	10.1	0.53	2.4	0.0014

Note. k_c refers to a scaling factor of the standard deviation of center mechanism of mRGC receptive field, k_s is a scaling factor of the standard deviation of surround mechanism of mRGC receptive field, w_c is a weighting factor between center and surround mechanism, ρ is a pooling exponent, P_0 is a baseline component representing the V1 masking when the background is uniform. For details, see Bradley et al. (13).

Table S3, Related to Fig. 5A. Studies of the cortical magnification factor in human V1 and the number of midget RGCs (mRGCs) underlying a 1-mm cortical distance derived from each study

Publications	**Cortical magnification factor function**	**Range of measurement or estimation**	**Number of mRGCs** (mean ± SD)
Cowey & Rolls (1974)	$1/(0.067\times Ecc+0.117)$ (function by Grüsser, 1995)	0°~30°	14.25 ± 0.40
Rovamo & Virsu (1979) *	Temporal: $7.99/(1+0.29\times Ecc+1.2e^{-5}\times Ecc^3)$ Nasal: $7.99/(1+0.33\times Ecc+7e^{-5}\times Ecc^3)$ Superior: $7.99/(1+0.42\times Ecc+1.2e^{-4}\times Ecc^3)$ Inferior: $7.99/(1+0.42\times Ecc+5.5e^{-5}\times Ecc^3)$	0°~80° 0°~60° 0°~45° 0°~60°	10.61 ± 0.53
Horton & Hoyt (1991) †	$17.3/(Ecc+0.75)$	–	11.25 ± 0.21
Grüsser (1995)	$1/(0.059\times Ecc+0.073)$	0°~30°	12.00 ± 0.14
Engel et al. (1997)	$15.87/Ecc$ (function by Popovic & Sjöstrand, 2001(14))	2°~12°	11.40 ± 0.61
Duncan & Boynton (2003)	$1/(0.065\times Ecc+0.054)$	1.5°~12°	12.74 ± 0.20
Dougherty et al. (2003)	$29.2/(Ecc+3.67)$	2°~12°	8.49 ± 0.76

Note. *Ecc* refers to retinal eccentricity. The number of midget RGCs (mRGCs) refers to the mean of the number of mRGCs per a 1-mm cortex distance averaged across 17 different eccentricities spanning from 4° to 20° eccentricities. SD refers to the standard deviation of the mean. * indicates that this study (15) estimated human cortical magnification factor from human RGC density data. † indicates that this study (16) derived human cortical magnification factor using the monkey cortical magnification data after correction. The other studies (17-21) relied on direct physiological or fMRI measurements of the human primary visual cortex.

References

1. Brainard DH (1997) The Psychophysics Toolbox. *Spat. Vis.* 10(4):433-436.
2. Pelli DG (1997) The VideoToolbox software for visual psychophysics: transforming numbers into movies. *Spat. Vis.* 10(4):437-442.
3. Wetherill GB & Levitt H (1965) Sequential estimation of points on a psychometric function. *Br. J. Math. Stat. Psychol.* 18:1-10.
4. Pelli DG, Palomares M, & Majaj NJ (2004) Crowding is unlike ordinary masking: distinguishing feature integration from detection. *J. Vis.* 4(12):1136-1169.
5. Toet A & Levi DM (1992) The two-dimensional shape of spatial interaction zones in the parafovea. *Vision Res.* 32(7):1349-1357.
6. Kwon M, Bao P, Millin R, & Tjan BS (2014) Radial-tangential anisotropy of crowding in the early visual areas. *J. Neurophysiol.* 112(10):2413-2422.
7. Petrov Y & Meleshkevich O (2011a) Asymmetries and idiosyncratic hot spots in crowding. *Vision Res.* 51(10):1117-1123.
8. Greenwood JA, Szinte M, Sayim B, & Cavanagh P (2017) Variations in crowding, saccadic precision, and spatial localization reveal the shared topology of spatial vision. *Proc. Natl. Acad. Sci. U. S. A.* 114(17):E3573-E3582.
9. Drasdo N, Millican CL, Katholi CR, & Curcio CA (2007) The length of Henle fibers in the human retina and a model of ganglion receptive field density in the visual field. *Vision Res.* 47(22):2901-2911.
10. Watson AB (2014) A formula for human retinal ganglion cell receptive field density as a function of visual field location. *J Vis* 14(7).
11. Bouma H (1970) Interaction effects in parafoveal letter recognition. *Nature* 226(5241):177-178.
12. Andriessen JJ & Bouma H (1976) Eccentric vision: adverse interactions between line segments. *Vision Res.* 16(1):71-78.
13. Bradley C, Abrams J, & Geisler WS (2014) Retina-V1 model of detectability across the visual field. *J. Vis.* 14(12):22-22.
14. Popovic Z & Sjöstrand J (2001) Resolution, separation of retinal ganglion cells, and cortical magnification in humans. *Vision Res.* 41(10-11):1313-1319.
15. Rovamo J & Virsu V (1979) An estimation and application of the human cortical magnification factor. *Exp Brain Res* 37(3):495-510.
16. Horton JC & Hoyt WF (1991) The representation of the visual field in human striate cortex. A revision of the classic Holmes map. *Arch. Ophthalmol.* 109(6):816-824.
17. Cowey A & Rolls ET (1974) Human cortical magnification factor and its relation to visual acuity. *Exp Brain Res* 21(5):447-454.
18. Grüsser O-J (1995) Migraine phosphenes and the retino-cortical magnification factor. *Vision Res.* 35(8):1125-1134.
19. Engel SA, Glover GH, & Wandell BA (1997) Retinotopic organization in human visual cortex and the spatial precision of functional MRI. *Cereb. Cortex* 7(2):181-192.
20. Duncan RO & Boynton GM (2003) Cortical magnification within human primary visual cortex correlates with acuity thresholds. *Neuron* 38(4):659-671.

21. Dougherty RF, *et al.* (2003) Visual field representations and locations of visual areas V1/2/3 in human visual cortex. *J Vis* 3(10):586-598.